

# Equations of state for ruthenium and rhodium

Damian C. Swift,<sup>1</sup> Thomas Lockard,<sup>1</sup> Olivier Heuzé,<sup>2</sup> Mungo Frost,<sup>3</sup> Siegfried Glenzer,<sup>3</sup> Kenneth J. McClellan,<sup>4</sup> Sebastien Hamel,<sup>1</sup> John E. Klepeis,<sup>1</sup> Lorin X. Benedict,<sup>1</sup> Philip A. Sterne,<sup>1</sup> and Graeme J. Ackland<sup>5</sup>

<sup>1</sup>*Lawrence Livermore National Laboratory, 7000 East Avenue, Livermore, California 94551, USA*

<sup>2</sup>*CEA/DAM-Île de France, Bruyères-le-Châtel, F-91297 Arpajon Cedex, France*

<sup>3</sup>*SLAC National Accelerator Laboratory, Menlo Park, California 94025, USA*

<sup>4</sup>*Los Alamos National Laboratory, MS G770, Los Alamos, New Mexico 87545, USA*

<sup>5</sup>*Department of Physics, University of Edinburgh, Edinburgh, EH9 3JZ, Scotland, UK*

(Dated: July 29, 2019 – LLNL-JRNL-780237)

Ru and Rh are interesting cases for comparing equations of state (EOS), because most general-purpose EOS are semi-empirical, relying heavily on shock data, and none has been reported for Ru. EOS were calculated for both elements using all-electron atom-in-jellium theory, and cold compression curves were calculated for the common crystal types using the multi-ion pseudopotential approach. Previous EOS constructed for these elements used Thomas-Fermi (TF) theory for the electronic behavior at high temperatures, which neglects electronic shell structure; the atom-in-jellium EOS exhibited pronounced features from the excitation of successive electron shells. Otherwise, the EOS matched surprisingly well, especially considering the lack of experimental data for Ru. The TF-based EOS for Ru may however be inaccurate in the multi-terapascal range needed for some high energy density experiments. The multi-ion calculations predicted that the hexagonal close-packed phase of Ru remains stable to at least 2.5 TPa and possibly 10 TPa, and that its  $c/a$  should gradually increase to the ideal value. A method was devised to estimate the variation in Debye temperature  $\theta_D$  from the cold curve, and thus estimate the ion-thermal EOS without requiring relatively expensive dynamical force calculations, in a form convenient for adjusting EOS or phase boundaries.  $\theta_D$  estimated in this way was similar to the result from atom-in-jellium calculations. We also predict the high-pressure melt loci of both elements.

## INTRODUCTION

Although they are relatively uncommon metals, Rh and Ru have several notable technological applications involving dynamic loading and elevated states of compression and heating.

Both Rh and Ru have important uses in strengthening alloys and as coatings resistant to corrosion. Their isotopes include some of the principal fission products of the actinides, and significant amounts build up as ingrowth in nuclear fuels and heat sources. For this reason, Rh and Ru are relevant in the reprocessing of nuclear waste, and their alloys are potential components of advanced nuclear fuels. There are situations where these materials may be subjected to compression, heating, and ablation, including aerospace applications of refractory alloys containing these elements, and accident scenarios involving future space fuels.

Both Ru and Rh have been proposed as a key component in experiments at the National Ignition Facility [1]. In these experiments, they are subjected to shocks of up to  $\sim 10$  TPa, and their subsequent expansion, along with that of lower-density components, is used to induce ramp loading in a sample to be studied [2]. An experiment using Rh has been performed, though not completely analyzed [3]. These pressures are far above any calibration of the equation of state (EOS) used in the design and interpretation of these rather expensive experiments, and for that matter well above almost all experimental data for any material. Relative shock Hugoniot exper-

iments have been performed to higher pressures using shocks driven by nuclear explosions [4], though with quite large uncertainties and without an accurate calibration of the impedance-matching standard materials. Absolute Hugoniot experiments have recently been demonstrated in this pressure range and above using laser-driven shocks [5, 6], but involve x-ray radiography, and are not yet feasible on samples of such high atomic number. This restriction is a motivation to evaluate the quality of existing EOS in this regime, and to improve them if possible.

In many experiments using ablation to induce loading, a variety of elements are employed as shields against unwanted x-ray heating from the ablation plasma, chosen on the basis of the expected source spectrum and deposition profile in the sample, for instance in x-ray diffraction experiments [7]. Although the accuracy EOS is often less important than for other components of the target, it may be crucial to predict correctly whether the shield melts, in order to identify the diffraction lines from the sample. For this reason, it is desirable to construct the melt locus of possible shield materials to high pressures.

Experiments have been performed on the intermetallic compound RuAl using laser ablation to induce a shock, and measuring the flow stress and spall strength. A model of Ru in the ablation plasma is needed to interpret these measurements [8].

There is a relative paucity of high pressure measurements on these elements. Very unusually for a non-toxic engineering metal element, we have found no shock data at all for Ru. The comparison between EOS for these

elements is thus an interesting test of the performance of theoretical techniques with limited experimental data to constrain models. We can make testable predictions of the high pressure properties of Ru in particular that are not informed by experimental measurements.

Here we construct wide-ranging EOS for Ru and Rh using average atom techniques most applicable in the fluid-plasma region, and assess their accuracy against published experimental measurements and also against multi-ion methods that perform better in the solid. We also use multi-ion electronic structure calculations to construct narrower-range EOS that apply better in the solid, and use these results to extend previous predictions of the stability field of the ambient phase to much higher pressures.

## PREVIOUS EQUATION OF STATE STUDIES

Currently, all accurate, general-purpose EOS are semi-empirical. The most usual thermodynamic approach is based on evaluating the Helmholtz free energy  $f$  as a function of mass density  $\rho$  and temperature  $T$ , decomposed into a cold compression curve  $f_c(\rho)$  along with thermal contributions for the ions  $f_i(\rho, T)$  and electrons  $f_e(\rho, T)$ . The pressure  $p$  and specific internal energy  $e$  are obtained by differentiation, and it is the resulting tabulations  $\{p, e\}(\rho, T)$  that constitute the EOS used in practice for studies of impacts and other hydrodynamic situations. Theoretical methods typically have difficulty in adequately reproducing the observed mass density at standard temperature and pressure (STP), and common practice has been to use the observed value, along with the compressibility and shock data, to calibrate algebraic functions for  $f_c$  by taking simplified forms for  $f_i$  in particular a Grüneisen form with a slowly-varying, analytic  $\Gamma(\rho)$ . Observations and predictions of phase changes, informed by electronic structure theory, have been used to make multiphase constructions primarily of  $f_c$  and  $f_i$ . For  $f_e$ , Thomas-Fermi (TF) theory [9] has been used most commonly, although some EOS have been constructed using treatments that, unlike TF, take account of electron shells.

For Rh, measurements of states along the principal shock Hugoniot have been reported for pressures up to  $\sim 0.2$  TPa [10]; for Ru there are none. Room-temperature compression measurements have been reported for both elements, but up to only 64 and 56 GPa for Rh and Ru respectively [11–14]. Data from presses have not been used as extensively as shock data for constructing EOS, because presses require a pressure calibrant whose uncertainty introduces another source of error whereas shock data can be absolute (and are the ultimate source of calibration for press data), and also because applications of EOS largely involve shock loading, so a direct calibration bypasses inaccuracies in treating the region between the

ambient isotherm and the principal Hugoniot.

The widely-used SESAME EOS library [15] includes a model for Rh [16], constructed by the usual semi-empirical approach using measurements of the principal shock Hugoniot to deduce the cold compression curve, and blending into a TF treatment at high temperatures. The LEOS library [17] has a model for Rh constructed similarly. It also includes a model for Ru constructed using the ‘quotidian EOS’ (QEOS) procedure [18] again employing TF theory at high temperatures, but using the measured mass density and sound speed at STP in the absence of shock data. No SESAME EOS has been constructed for Ru.

Theoretical studies of Ru and Rh have been included among extensive research on the transition elements [19–21], although we have found no comparisons made with existing EOS models, and a relative lack of work on the thermal EOS. In most cases, no EOS was constructed, and results were insufficient for constructing EOS into the fluid and plasma regimes. For Rh, a mean field approach has been used to construct the EOS for the solid [22], though the resulting EOS was a poor match to mechanical properties such as observed shock Hugoniot states. These calculations suggested that electron-thermal energy is unusually large at  $\sim 30\%$  of the ion-thermal energy above 800 K. The derivation of the electron-thermal energy was not described in detail, but was apparently a free electron gas, which is unlikely to be accurate over a wide range of states. Studies using tight-binding theory [20] reproduced the observed crystal structure of Ru and Rh to the limits of published data ( $\sim 50$  GPa), and predicted that their ambient structures would persist to at least 0.4 and 0.5 TPa respectively.

Further work is clearly needed to test and constrain EOS into the high energy density regime. A challenge is that the most rigorous techniques available are both computationally expensive and not strictly valid over the full range from STP to states of high compression and heating, and subsequent expansion. Ru and Rh have atomic numbers 44 and 45 respectively, and so the electron-thermal EOS must dominate over the ion-thermal under shock loading or heating sufficient to start ionizing the weakly-bound outer electrons. The most rigorous approach to calculating electronic states is quantum Monte Carlo, such as path integral Monte Carlo (PIMC) [23] which accounts for the antisymmetry of the electron wavefunctions under particle exchange. However, PIMC calculations have not been reported yet for such high atomic numbers. In PIMC, the ion-thermal energy is approximated by the high temperature limit of an ideal monatomic gas,  $\frac{3}{2}k_B T$  per atom, which is not appropriate in condensed phases. At lower temperatures, quantum molecular dynamics (QMD) has been extensively used, in which the effects of exchange and correlation on the wavefunctions are estimated using Kohn-Sham density functional theory (DFT), the inner electrons of

each atom are subsumed into a pseudopotential rather than treated explicitly, and ion trajectories are simulated from Hellmann-Feynman forces on the ions [24]. The QMD treatment of the electrons is less rigorous than in PIMC and the converse for the ions. However, the ion trajectories are nevertheless classical, and do not account for the quantum mechanical ion effects of zero-point motion and quenching of vibrational modes at low temperature. Both of these effects can be accounted for by using Hellmann-Feynman forces in DFT to calculate phonon modes for solid phases only [25], although, when constructing an EOS, integrating over the complete phonon spectrum means that the detailed contribution from each mode is lost, and it is often adequate to describe the ion-thermal free energy in terms of a Debye model [26] in which the Debye temperature  $\theta_D$  depends on compression. Formally, since the ion-thermal heat capacity must vary between zero at low temperatures and  $3k_B$  per atom when all the phonon modes are fully excited, it is always possible to express the ion-thermal free energy using a Debye model which depends on both density and temperature  $\theta_D(\rho, T)$ . In fact, as the bulk modulus of matter can also be regarded as an integral over vibrational modes, it is also possible to estimate the ion-thermal free energy from the compressibility without explicitly calculating any ion-thermal motion [27], although ion-thermal energies deduced in this way from the cold compression curve have been found to be inaccurate.

It has recently been shown that results from PIMC and QMD for elements can be reproduced by all-electron DFT calculations of spherically-symmetric wavefunctions about an ion situated in a cavity within a uniform charge density ‘jellium’ representing neighboring atoms [28–30]. This atom-in-jellium approach [31] requires much less computation than three-dimensional, multi-ion simulations, and the ion-thermal treatment, based on calculating the Debye temperature [32] has been extended to account for the decrease in heat capacity from 3 to  $\frac{3}{2}k_B$  per atom as the ions cease to be bound by their neighbors at high temperatures [33]. The atom-in-jellium model is a gross simplification of the interaction between neighboring nuclei, and the calculation of ion-thermal energy is based on a crude average vibration energy compared with QMD and phonon treatments, but its use of a Debye-like ion-thermal model captures both the zero-point energy and the freezing of vibrational modes. These attributes are likely to be masked by the relative inaccuracy of atom-in-jellium at low pressures, but they are potentially significant in cool, compressed states as can be accessed using ramp loading [34]. Despite significant inaccuracies around STP, atom-in-jellium calculations do indeed seem to perform well for ramp compression into the terapascal regime as is possible at the National Ignition Facility [35]. We had previously presumed that this consistency mostly reflected the difficulty of making experimental measurements accurate enough to show the

inaccuracy of the atom-in-jellium model at these high pressures and internal energies, but recent QMD studies on states of warm dense matter states have suggested that ions interact effectively through a screened Yukawa potential [36], and thus the atom-in-jellium model may actually be close to accurate in this regime, as opposed merely to being relatively less inaccurate.

## EQUATION OF STATE CALCULATIONS

The principal motivation for this study was to test and improve EOS for use in high energy density (HED) experiments, and here we pay closest attention to theoretical calculations valid on terapascal and electron-volt scales, and higher. Thus we used the atom-in-jellium model to construct wide-range EOS in the expectation that they would be relatively inaccurate around STP. Given the interesting observations that Ru and Rh retain their ambient structure (hexagonal close packed, hcp, and face-centered cubic, fcc, respectively) to the highest pressures reported experimentally [12, 14] or theoretically [20], this suggests their potential use as pressure calibrants in diffraction experiments. With the development of ramp loading and *in situ* diffraction, such experiments are now routinely performed in large laser facilities into the terapascal range [37], and so we used multi-ion pseudopotential calculations of the cold compression curve for several crystal structures as an indication of whether phase transitions might be expected at pressures above those investigated previously. We used these cold curves to estimate the Grüneisen parameter and hence, combined with the experimentally-determined  $\theta_D$ , an estimate of the ion-thermal contribution to the EOS, providing greater accuracy around STP in the solid.

### Atom-in-jellium

Atom-in-jellium simulations were performed using the same prescription as developed previously for other elements [30, 33]. For each element, atom-in-jellium calculations were made over a range and density of states suitable for a general-purpose EOS: mass density  $\rho$  from  $10^{-4}$  to  $10^3\rho_0$  with 20 points per decade, and temperature  $T$  from  $10^{-3}$  to  $10^5$  eV with 10 points per decade. The reference mass density  $\rho_0$  was chosen to be the observed STP value; this choice is purely a convenience in constructing tabular EOS, where it is useful for the tabulation to include the starting state to reduce the sensitivity to interpolating functions. The EOS were not adjusted to reproduce any empirical data.

As was found in the previous study [30], the electronic wavefunctions were computed reliably down to 10 K or less for densities corresponding to condensed matter, and to 100 K or less for densities down to 0.1% of the ambient

solid. At lower densities, calculations were completed successfully only for temperatures of several eV or more.

The results of the atom-in-jellium calculations were, for each state of mass density  $\rho$  and temperature  $T$ , electronic contributions to the Helmholtz free energy  $f$ , the estimated Debye temperature  $\theta_D$ , the mean square displacement of the atom as a fraction of the Wigner-Seitz radius  $f_d$ , and the ionic contribution to  $f$  using the generalized Debye model with asymptotic ionic freedom [30, 33]. The total electronic energy was used: it was taken to include the cold compression energy and was not adjusted to extract a separate electron-thermal energy. The fields were post-processed to fill in states where the calculation failed to converge properly, using polynomial interpolation from surrounding states. For each state, the total Helmholtz free energy  $f$  was calculated, and then differentiated using a quadratic fit to the three closest states in  $\rho$  to determine the pressure  $p(\rho, T)$  in tabular form. Similarly, quadratic fits in  $T$  were differentiated to find the specific entropy  $s$  and hence the specific internal energy  $e(\rho, T)$  in tabular form. These tabulated functions comprise an EOS in SESAME or LEOS form.

To help assess the accuracy of the ion-thermal energy, we considered the predicted Debye temperatures  $\theta_D$ . As described previously [30, 32, 33], the calculation proceeds by using perturbation theory to calculate the force constant for displacement of the ion from the center of the cavity in the jellium, and hence the Einstein temperature  $\theta_E$ .  $\theta_D$  is then deduced from  $\theta_E$  in two alternative ways, by equating either the energy or the mean amplitude of displacement.  $\theta_D$  is calculated as a function of both  $\rho$  and  $T$ , although its precise value is important only when  $T \simeq \theta_D$ . For this reason, we have previously calculated an effective  $\theta_D(\rho)$  by taking the locus  $\theta_D(\rho, T) = T$  [30]. The value calculated this way can be significantly different than the value along the cold compression curve,  $\theta_D(\rho, 0)$ , or as close to the cold curve as can be reached using atom-in-jellium computations.

The atom-in-jellium calculations included the mean amplitude  $u$  of ionic oscillations as a function of the Wigner-Seitz radius  $r_{WS}$ . The ratio was used to predict the variation of melt temperature with compression and hence, using the EOS, the melt locus as a function of pressure, as was reported previously for Al and Fe [38].

### Multi-atom pseudopotential

Three-dimensional multi-ion simulations were performed using non-local pseudopotentials to represent the inner electrons on each atom, and a plane wave expansion to represent the outer electrons, solving the Kohn-Sham DFT equations [39–42] with respect to the Schrödinger Hamiltonian, and thus calculating the ground state energy along with forces and stresses via the Hellmann-

Feynman theorem, for a series of different values of the lattice parameters.

The pseudopotentials used were generated by the Troullier-Martins method [43] with the inner 36 electrons (i.e. the closed shells of Kr) treated as core and the outer 8 (Ru) or 9 (Rh) treated explicitly as valence. The wavefunction was evaluated at  $10^3$  regularly-spaced points in reciprocal space, reduced by the symmetry of the crystal lattice [44]. A plane-wave cutoff of 2000 eV was sufficient to converge the ground states to  $\sim 1$  meV/atom or better.

For non-cubic structures, the lattice vectors giving any specific stress, such as isotropic, were predicted by assigning a fictitious mass to the parameters and evolving them for short periods under the instantaneous Hellmann-Feynman stress. The rate of change of each parameter was reset to zero before each iteration, so this procedure is effectively a critically-damped dynamics. The method used was a variant of one developed previously [45], modified to check the degree of convergence of the electron states and stress automatically, rather than performing a set number of iterations. We found that the number of iterations needed to reach convergence could sometimes vary by a factor of several between calculations at adjacent lattice parameters, highlighting the importance of this adaptive method in obtaining consistently-converged solutions.

### Semi-empirical ion-thermal energy

The multi-ion compression curves were used to estimate the ion-thermal EOS simply, without having to perform the relatively laborious procedure of constructing the phonon density of states as we have in previous work [25, 46]. We consider this justified as, in the solid, the ion-thermal contribution is a relatively small correction to the dominant contribution of the cold curve to the EOS, and in the present work we are not concerned with subtle effects on phase boundaries where small corrections may matter.

We used the Burakovsky and Preston’s form [47] of the relationship between the Grüneisen parameter  $\Gamma(\rho)$  and the cold curve,

$$\Gamma(\rho) = \frac{\frac{B'(\rho)}{2} - \frac{1}{6} - \frac{t}{2} \left[ 1 - \frac{p(\rho)}{3B(\rho)} \right]}{1 - \frac{2t}{3} \frac{p(\rho)}{B(\rho)}} \quad (1)$$

where  $p$  is the pressure,  $B$  the bulk modulus, and  $B'$  its pressure derivative. The ion-thermal EOS has been found to be represented most accurately by a value of  $t$  which increases from 0 to 2 with compression [47]. For simplicity, we chose  $t = 2$  to select the Vashchenko-Zubarev relation [48], as the ion-thermal contribution to the principal shock Hugoniot is in any case smaller at lower pressure.

The Grüneisen parameter is the logarithmic derivative

of the Debye temperature,

$$\Gamma(\rho) = \frac{\rho}{\theta_D} \frac{d\theta_D}{d\rho}, \quad (2)$$

and so the Debye temperature can be expressed as

$$\theta_D(\rho) = \theta_D(\rho_r) G(\rho) / G(\rho_r) \quad (3)$$

where

$$G(\rho) \equiv \exp \int^{\rho} \frac{\Gamma(\rho')}{\rho'} d\rho' \quad (4)$$

and  $\rho_r$  is some reference density.

The electronic structure calculations gave the ground state energy and, by the Hellmann-Feynman theorem,  $p$ , at each of a series of mass densities  $\rho$ . In order to perform the further differentiation necessary to calculate  $B$  and  $B'$ , the cold curve was fitted with analytic functions. Several functions were tried, and a modified version of the Vinet form [49] was found to fit the cold curve over the widest range:

$$e(\rho) = e_c \phi[a(\rho)] + e_0 : \phi(a) = - \left( 1 + a + \frac{1}{20} a^3 \right) \quad (5)$$

where

$$a(\rho) = \frac{(\rho_0/\rho)^{1/3} - 1}{l}, \quad \eta(\rho) = \frac{\rho}{\rho_0} - 1. \quad (6)$$

The fitting parameters are  $l$ ,  $\rho_0$ ,  $e_c$ , and  $e_0$ . The modifications to remove the need for material-specific constants such as the atomic weight, used to calculate the Wigner-Seitz radius, and thus give a more convenient relation for describing arbitrary  $e(\rho)$  data, given that the scaling parameter  $l$  is fitted to reproduce the data in any case. In some cases, such as Rh, the range of the fit can be extended by making  $l$  a function of  $\rho$ , such as a low-order polynomial.

One advantage of this procedure over a more detailed phonon calculation resulting in a tabular EOS is that it can more readily be adjusted to better match other data. Adjustments can be made conveniently to the parameters fitting the cold curve, and to the reference value of the Debye temperature,  $\theta_D(\rho_r)$ .

When used over the full range of states considered here, we generally had to split the fit into low and high pressure regions, with a different set of parameters for each.

## RESULTS

Atom-in-jellium EOS, and multi-atom pseudopotential cold curves, were constructed for each element as above. In each case, the EOS was analyzed to extract the ambient isotherm and isochore, and to deduce the principal isentrope and principal shock Hugoniot, for comparison with previous EOS and experimental measurements.

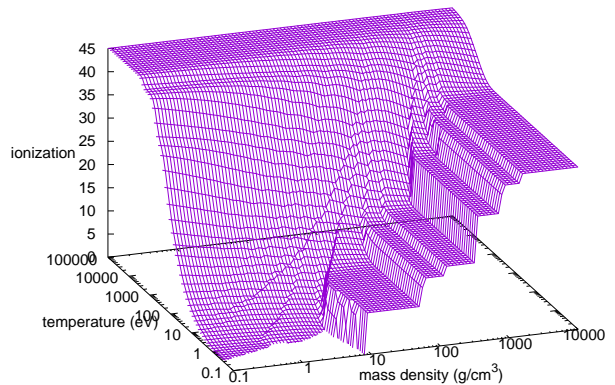


FIG. 1: Atom-in-jellium prediction of ionization in rhodium.

These loci are characteristic of different conditions to which matter may be subjected: the isotherm and isentrope are limiting cases of compression at low rates, the isochore is representative of ablation, and the Hugoniot is the locus for high loading rates. On the scale of the graphs below, the principal isentrope was not distinguishable from the ambient isotherm, and is not shown.

To accommodate the wide ranges calculated, we plot graphs in log space. This turns out to be reasonable: lines are almost coincident when quantities match to within a few percent, which is typical for what constitutes agreement in high pressure physics, while being convenient for quantifying the difference between models that differ significantly.

## Rhodium

The thermal ionization calculated using the atom-in-jellium method was broad with smeared-out shell features, whereas ionization in response to compression (commonly, if loosely, referred to as ‘pressure ionization’) was calculated to occur in distinct steps, a characteristic behavior of the average atom treatment (Fig. 1). However, the pressure ionization steps did not manifest as an abrupt change of slope in the ambient isotherm. Ionization can be used as an indication of when pseudopotentials may become invalid. In the atom-in-jellium calculations, the Kr-like shells remained bound up to 50 g/cm<sup>3</sup> and below 7 eV.

At the observed STP mass density of 12.41 g/cm<sup>3</sup>, the atom-in-jellium EOS gave a pressure of -27 GPa and the multi-ion pseudopotential calculation gave 15 GPa. These discrepancies are typical for the respective techniques: somewhat larger than usual for pseudopotential calculations, and less than usual for atom-in-jellium. The

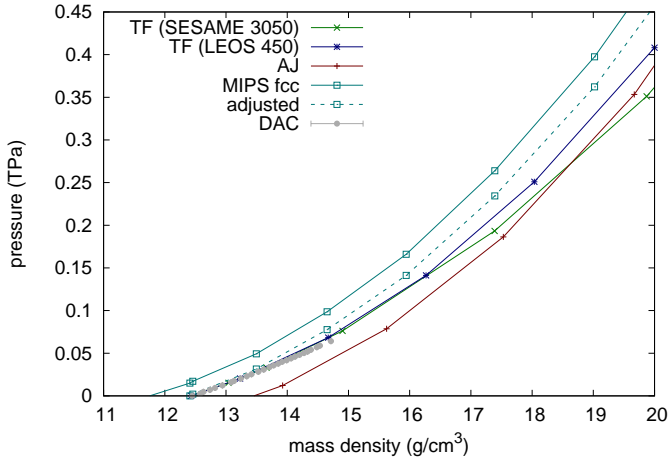


FIG. 2: Low pressure ambient isotherm of rhodium, showing atom-in-jellium (AJ) and Thomas-Fermi (TF) based EOS, multi-ion pseudopotential calculations (MIPS), diamond anvil cell (DAC) measurements [12], and pseudopotential calculations adjusted to match the mass density observed at STP.

ambient isotherms lay correspondingly below and above reported diffraction data from diamond anvil compression [12]. To obtain a more accurate EOS at low pressures, we have previously adjusted the energy obtained from electronic structure calculations to reproduce the observed STP state [25, 50]. Applying this correction to the pseudopotential states brought the isotherm into better agreement with the data, though the calculations lay increasingly above the data with pressure. Isotherms from the general-purpose TF-based EOS deviated above  $\sim 0.15$  TPa. Measurements at higher pressure would be valuable. (Fig. 2.)

Over a wider pressure range, the isotherm predicted from atom-in-jellium was very consistent with the semi-empirical TF-based EOS LEOS 450; the similarly-constructed SESAME 3050 was up to 15% softer. (Fig. 3.)

The atom-in-jellium isochore closer to the SESAME EOS up to  $\sim 10$  eV, though different from both and showing ionization of successive electron shells. The atom-in-jellium EOS should be as reasonable as either of the semi-empirical EOS to below 30 GPa, when ionic contribution dominates. This is a remarkable degree of consistency of ion-thermal pressure from the atom-in-jellium model. At higher temperatures relevant to ablation in laser-driven experiments, all the EOS were close to each other. (Fig. 4.)

The atom-in-jellium Hugoniot passed among the experimental measurements around 0.2 TPa. Below 0.1 TPa, it fell well below the experiments, reflecting the inaccuracy of atom-in-jellium around STP. The atom-in-jellium Hugoniot was  $\sim 10\%$  stiffer than the semi-empirical LEOS 450 at a few terapascals, remarkably

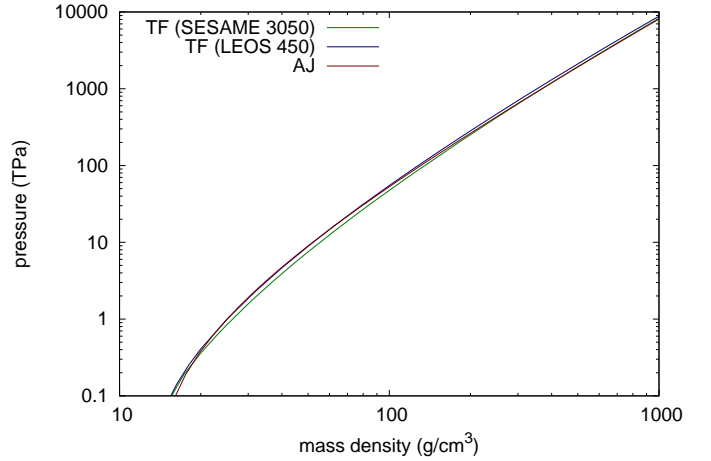


FIG. 3: Ambient isotherm of rhodium from atom-in-jellium (AJ) and Thomas-Fermi (TF) based EOS.

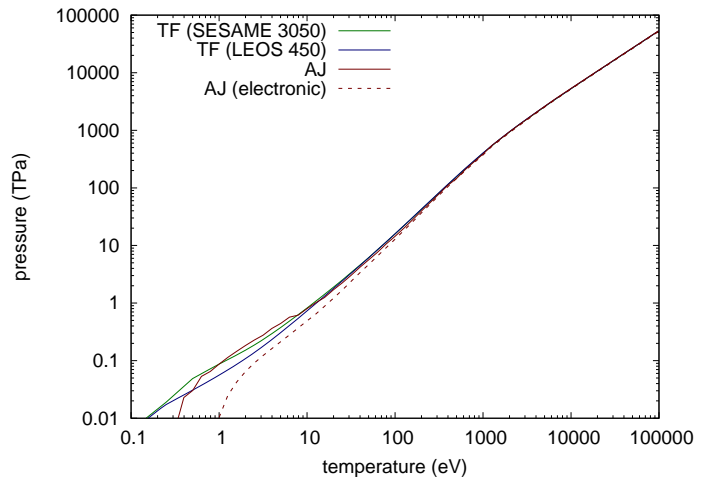


FIG. 4: Ambient isochore of rhodium from atom-in-jellium (AJ) and Thomas-Fermi (TF) based EOS.

close to it over  $\sim 8-70$  TPa, and then exhibited shell ionization features at higher pressures, not predicted with TF models. The other TF-based semi-empirical EOS, SESAME 3050, generally lay  $\sim 10-20\%$  below the atom-in-jellium and LEOS Hugoniot. (Fig. 5.)

The pseudopotential calculations predicted that the bcc structure was energetically unfavorable over the full compression range considered, but that fcc and hcp lay much closer together. Fitting a modified Vinet function to the fcc calculations, which was valid to at least  $45 \text{ g/cm}^3$ , the hcp structure was found to lie at a higher energy even when  $c/a$  was optimized, and the calculations were thus consistent with Rh remaining in the fcc structure to at least 10 TPa, which is the limit beyond which the pseudopotential was likely to become invalid.

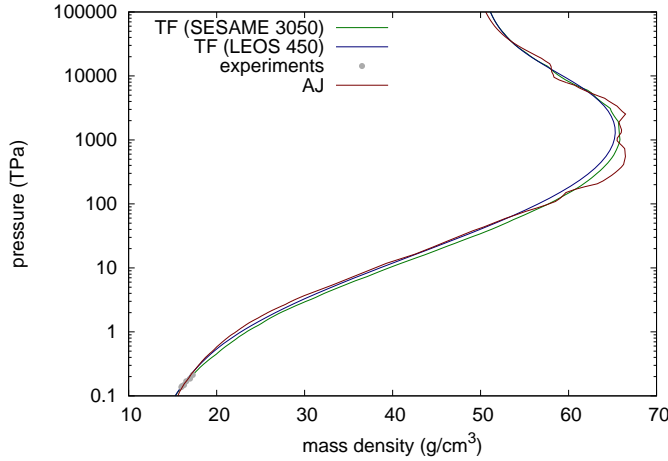


FIG. 5: Principal Hugoniot of rhodium from atom-in-jellium (AJ) and Thomas-Fermi (TF) based EOS.

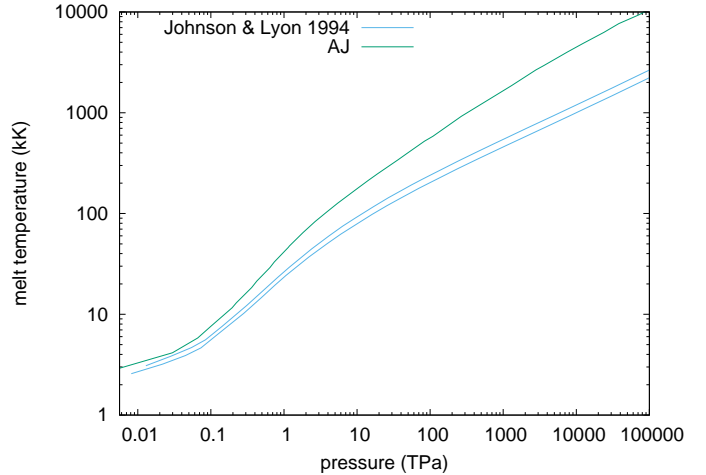


FIG. 7: Melt locus for Rh predicted from atom-in-jellium oscillations (AJ) and using a modified Lindemann model [51].

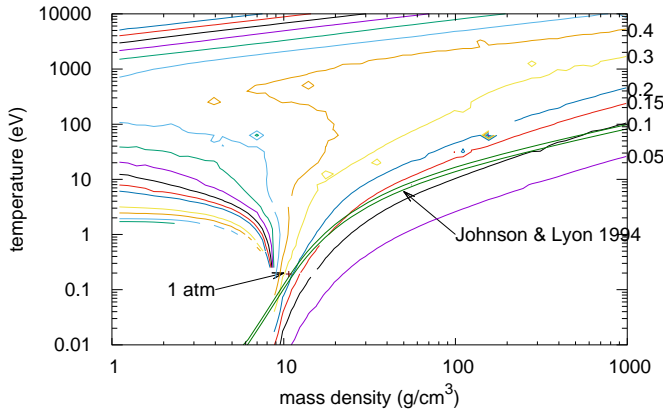


FIG. 6: Contours of mean ionic displacement of Rh divided by the Wigner-Seitz radius, along with the observed one-atmosphere melt point and a modified Lindemann prediction of the melt locus (solidus and liquidus) [51].

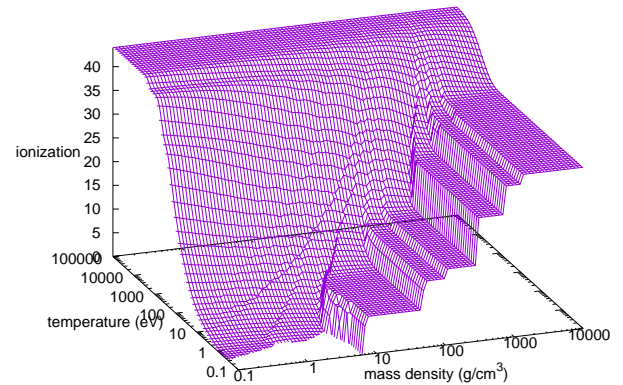


FIG. 8: Atom-in-jellium prediction of ionization in ruthenium.

This result extends the previous study using tight binding theory [20] by a factor  $\sim 20$  in pressure.

One-atmosphere melting of Rh lay close to the ion oscillation contour with an amplitude of  $u/r_{WS} \simeq 0.2$ . Taking this contour to extrapolate to other compressions, we predicted the melt locus as a function of mass density and, using the EOS, a function of pressure. The melt locus of Rh has been predicted previously using a modified Lindemann criterion in which the Grüneisen parameter is used to extrapolate from the one-atmosphere melt temperature by integration [51]. The atom-in-jellium prediction lay significantly above the older model. (Figs 6 and 7.)

## Ruthenium

Atom-in-jellium predictions of ionization in Ru exhibited features very similar to those in Rh. The Kr-like shells remained bound to above  $40 \text{ g/cm}^3$  and below  $10 \text{ eV}$  (Fig. 8).

At the observed STP mass density of  $12.45 \text{ g/cm}^3$ , the atom-in-jellium EOS gave a pressure of  $-39 \text{ GPa}$  and the multi-ion pseudopotential calculation gave  $16 \text{ GPa}$ : similar discrepancies as for Rh. The ambient isotherms lay correspondingly below and above reported diffraction data from diamond anvil compression [14]. To obtain a more accurate EOS at low pressures, we have previously adjusted the energy obtained from electronic structure calculations to reproduce the observed STP state

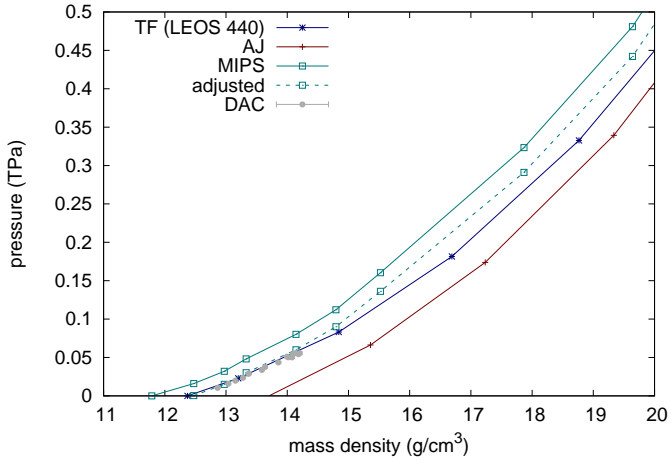


FIG. 9: Low pressure ambient isotherm of ruthenium, showing atom-in-jellium (AJ) and Thomas-Fermi (TF) based EOS, multi-ion pseudopotential calculations (MIPS), diamond anvil cell (DAC) measurements [14], and pseudopotential calculations adjusted to match the mass density observed at STP.

[25, 50]. Applying the equivalent correction [25, 50] as for Rh to bring the pseudopotential calculations into agreement with the STP state, the adjusted isotherm matched the diamond anvil data well. Interestingly, the isotherm deviated from the TF-based LEOS 440, the only semi-empirical EOS available, starting just above the limit of diamond anvil data; measurements to higher pressure would be valuable. (Fig. 9.)

Over a wider pressure range, the ambient isotherm and isochore from atom-in-jellium were remarkably similar to that from the TF-based LEOS 440, though not identical. The agreement between the isotherms is notable as, at low pressures, semi-empirical EOS are dominated by fitting to shock data, which was non-existent for Ru. (Figs 10 and 11.)

Similarly for the principal Hugoniot, the results from atom-in-jellium were very similar to the semi-empirical EOS, indicating that extrapolation from ambient using the bulk modulus was surprisingly accurate. Counterintuitively, given the agreement to  $\sim 70$  TPa in Rh, for Ru the atom-in-jellium Hugoniot fell below the TF model around 3 TPa, the deviation increasing to  $\sim 10\%$  in mass density and  $\sim 20\%$  in pressure, before the pronounced effects of shell ionization gave larger differences above 100 TPa. (Fig. 12.)

Using the three-dimensional, multi-ion pseudopotential method, the lattice parameters for states of isotropic stress were calculated as described above. Lattice vectors were sought for a sequence of increasing pressures, using the previous lattice vectors as the initial guess for the next higher pressure. Converged to finite accuracy, the lattice parameters exhibited clear trends, but also showed

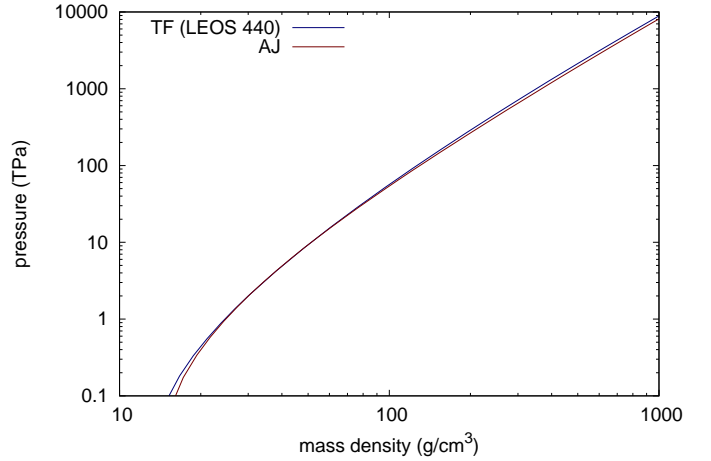


FIG. 10: Ambient isotherm of ruthenium from atom-in-jellium (AJ) and Thomas-Fermi (TF) based EOS.

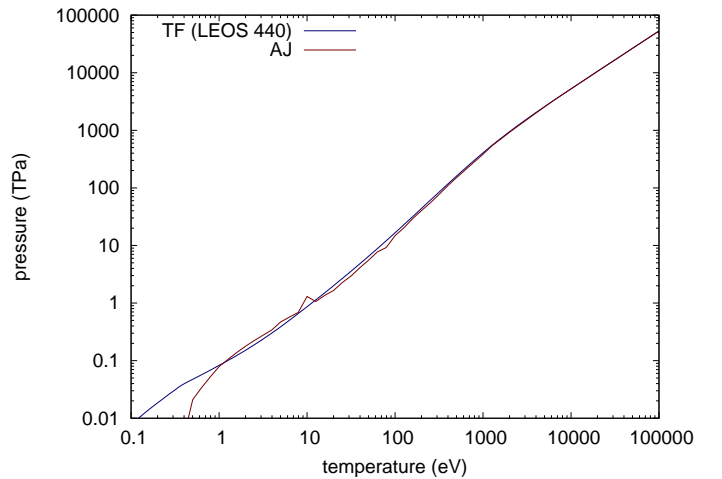


FIG. 11: Ambient isochore of ruthenium from atom-in-jellium (AJ) and Thomas-Fermi (TF) based EOS.

numerical noise. The hcp  $c/a$  ratio was calculated to be 1.583 at zero pressure, close to the observed value of 1.584 [14] and to the value 1.58 found using full-potential linearized augmented plane wave (FLAPW) calculations [20].  $c/a$  was predicted to rise to the ideal value of  $\sqrt{8/3}$  around 10 TPa, and then to fall for higher pressures. However, above 10 TPa, the density reaches the range where the atom-in-jellium calculations predicted pressure-ionization of the  $4p$  shell, and so a deeper pseudopotential should be used. The rate of increase of  $c/a$  with pressure was locally faster than observed in diamond anvil cell experiments, but had a similar magnitude [14]. (Fig. 13.)

The pseudopotential calculations predicted that hcp remained the lowest energy structure of those considered,



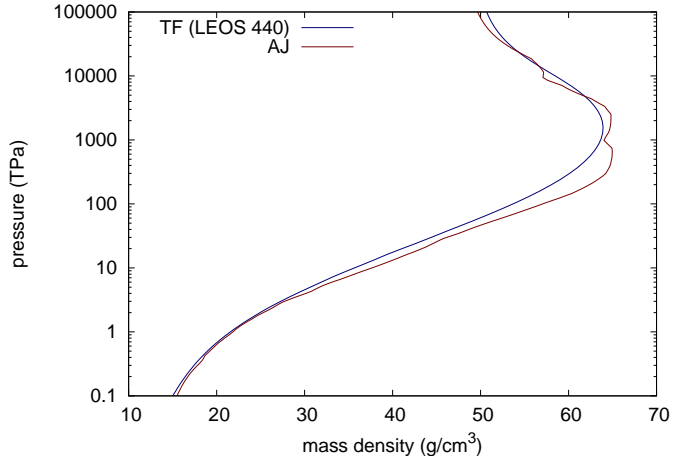


FIG. 12: Principal Hugoniot of ruthenium from atom-in-jellium (AJ) and Thomas-Fermi (TF) based EOS.

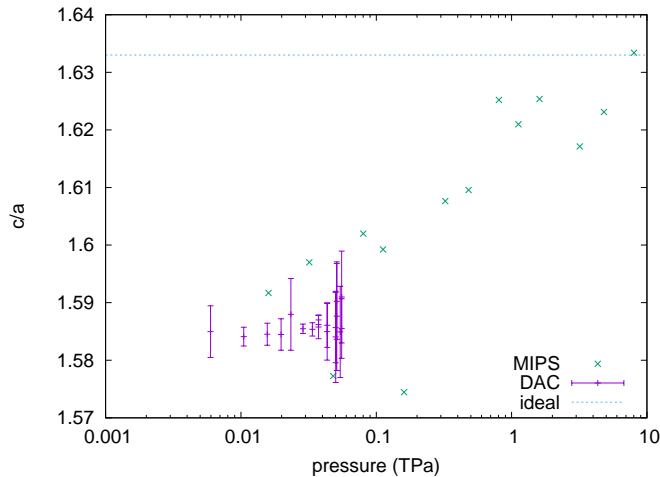


FIG. 13:  $c/a$  for hcp ruthenium, from multi-ion pseudopotential (MIPS) calculations, compared with diamond anvil cell (DAC) measurements [14].

up to the highest compression calculated of  $87.5 \text{ g/cm}^3$  or  $80.1 \text{ TPa}$ . This result was obtained allowing the hcp structure to relax, i.e.  $c/a$  to vary; with  $c/a$  held constant at the observed STP value, fcc was calculated to become more stable between  $0.42$  and  $2.26 \text{ TPa}$ . Above  $2.5 \text{ TPa}$ , the energies of fcc and the relaxed hcp structures were very close, so the prediction of hcp stability may be unreliable, and above  $10 \text{ TPa}$  the prediction should be regarded as unreliable since the calculations did not account for ionization of the inner shells. The bcc structure was calculated to have a significantly higher energy than hcp or fcc over full range considered, consistent with the FLAPW results at lower pressures [20].

Debye temperatures  $\theta_D$  were estimated from the hcp

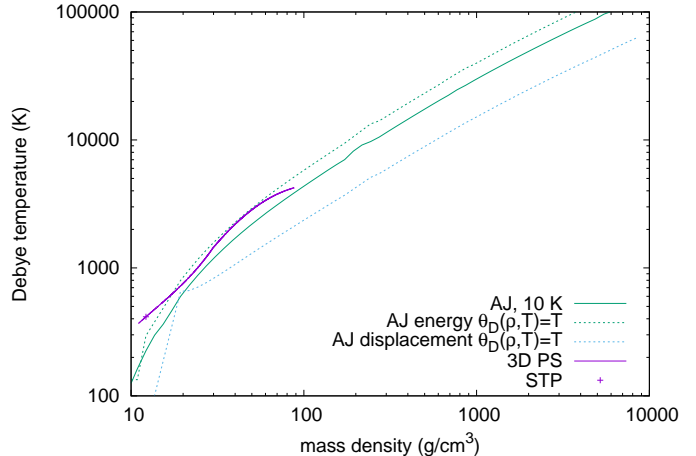


FIG. 14: Debye temperature of ruthenium, from atom-in-jellium calculations and also inferred from the STP value using the Grüneisen  $\Gamma$  calculated from the 3D pseudopotential calculations.

cold curve, using Eq. 3 to predict the variation from the STP value of  $415 \text{ K}$  [52], and compared with the alternative atom-in-jellium prescriptions for  $\theta_D$ . The atom-in-jellium  $\theta_D(\rho, 10 \text{ K})$ , effectively the cold curve dependence, was indistinguishable using the energy and displacement prescriptions. The loci calculated as  $\theta_D(\rho, T) = T$  in each case, which should be more accurate as a representation of the full  $\theta_D(\rho, T)$ , varied from the cold curve dependence in opposite directions. Apart from the region below  $20 \text{ g/cm}^3$ , where the atom-in-jellium  $\theta_D$  fell well below, the  $\theta_D$  estimated from the multi-ion simulations lay between the cold-curve and energy-based effective  $\theta_D$  model, which was higher than the cold variation, and closer to the effective  $\theta_D$ . At higher compressions, where the pseudopotential was expected to become invalid,  $\theta_D$  was predicted to flatten out; this result is probably not reliable. This comparison suggests that  $\theta_D$  calculated in these very different ways can be consistent, at least at the few percent level, and that the energy-based atom-in-jellium calculation of  $\theta_D$  may be the better. (Fig. 14.)

One-atmosphere melting of Ru also lay close to the ion oscillation contour with an amplitude of  $u/r_{\text{WS}} \simeq 0.2$ . As for Rh, we used this contour to extrapolate to other pressures. We attempted to fit the Simon relation [53] to the locus; it was not able to fit the full range of the calculation, but was a reasonable fit in each of three regions demarcated by  $10$  and  $1000 \text{ TPa}$ . Interestingly, these points correspond to the most abrupt changes in pressure ionization, suggesting that the melt locus appears to be more directly sensitive to changes in ionization than the isotherm. (Figs 15 and 16.)

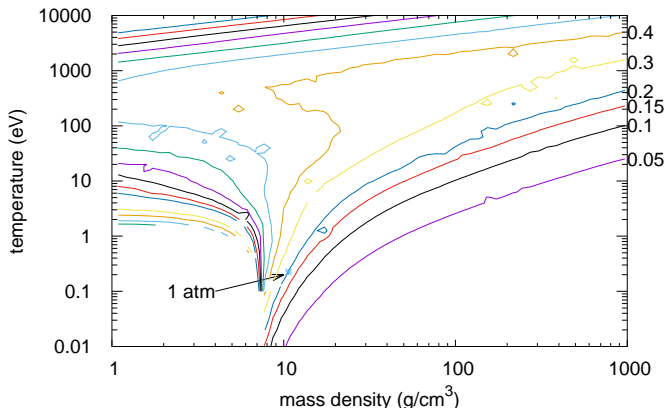


FIG. 15: Contours of mean ionic displacement of Ru divided by the Wigner-Seitz radius, along with the observed one-atmosphere melt point.

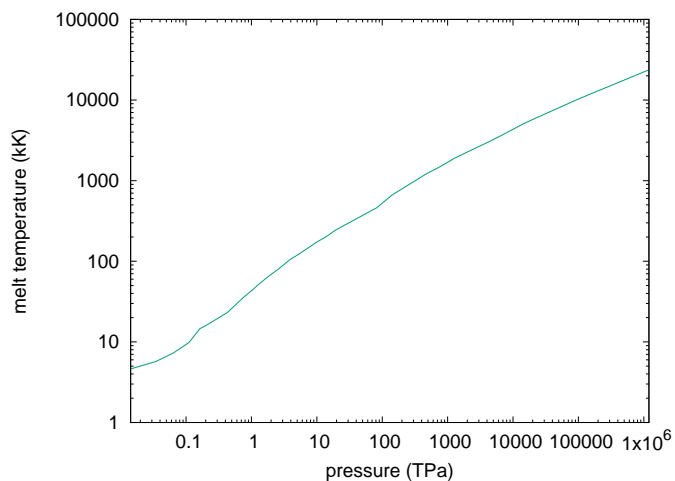


FIG. 16: Melt locus for Ru predicted from jellium oscillations.

## CONCLUSIONS

Wide-ranging EOS, intended principally for high energy density applications, were constructed self-consistently for Ru and Rh using atom-in-jellium theory. In Rh, for which measurements of the shock Hugoniot have been reported and used previously in the construction of general-purpose EOS, our *ab initio* EOS gave very similar behavior, except that our Hugoniot exhibited features corresponding to the ionization of successive electron shells which were absent in the previous EOS based on TF theory. In Ru, for which no shock Hugoniot measurements have been reported, our EOS was significantly more compressible than the only general-purpose EOS known, suggesting that this EOS gives shock pressures

that are roughly 40% too high, or mass densities that are about 10% too low, in the range  $\sim 4$ -500 TPa. Interestingly, in the regime where the semi-empirical EOS would have been guided by shock data, it agreed very well with the *ab initio* EOS; the difference arose at higher shock pressures where the semi-empirical EOS transitioned to the TF model. These comparisons indicate that the QEOS procedure used to construct the semi-empirical EOS in general works extremely well. Nevertheless, this difference in EOS between two adjacent transition elements highlights the potential inaccuracy of semi-empirical EOS constructed given limited shock data, or in its absence, and is a motivation to collect additional data in the terapascal range and above.

Cold compression curves were predicted for the common crystal structures using three dimensional pseudopotential calculations. Ru was predicted to remain hcp to at least 2.5 TPa, probably 10 TPa, and possibly higher, although the pseudopotentials used to calculate these cold curves are likely to be inaccurate at higher pressures.  $c/a$  matched the observed value at STP, and was predicted to increase toward the ideal value at  $\sim 10$  TPa; the initial rate of increase matched existing diamond anvil results. Rh was predicted to remain fcc to at least 10 TPa. The predicted absence of phase transitions in both elements suggests their possible use as a pressure calibrant in high-pressure diffraction experiments.

Melt loci were predicted for both elements; the result for Rh lay significantly above the previous prediction.

## Acknowledgments

This work was performed under the auspices of the U.S. Department of Energy under contract DE-AC52-07NA27344.

- 
- [1] S.T. Prisbrey, unpublished.
  - [2] S.T. Prisbrey, H.-S. Park, B.A. Remington, R. Cavallo, M. May, S.M. Pollaine, R. Rudd, B. Maddox, A. Comley, L. Fried, K. Blobaum, R. Wallace, M. Wilson, D. Swift, J. Satcher, D. Kalantar, T. Perry, E. Giraldez, M. Farrell, and A. Nikroo, *Phys. Plasmas* **19**, 056311 (2012).
  - [3] H.-S. Park, private communication.
  - [4] C.E. Ragan III, *Phys. Rev. A* **29**, 1391 (1984).
  - [5] T. Döppner, D.C. Swift, A.L. Kritcher, B. Bachmann, G.W. Collins, D.A. Chapman, J. Hawreliak, D. Kraus, J. Nilsen, S. Rothman, L.X. Benedict, E. Dewald, D.E. Fratanduono, J.A. Gaffney, S.H. Glenzer, S. Hamel, O.L. Landen, H.J. Lee, S. LePape, T. Ma, M.J. MacDonald, A.G. MacPhee, D. Milathianaki, M. Millot, P. Neumayer, P.A. Sterne, R. Tommasini, R.W. Falcone, *Phys. Rev. Lett.* **121**, 025001 (2018).
  - [6] D.C. Swift, A. L. Kritcher, J.A. Hawreliak, A. Lazicki, A. MacPhee, B. Bachmann, T. Döppner, J. Nilsen,

- G.W. Collins, S. Glenzer, S.D. Rothman, D. Kraus, and R.W. Falcone, *Rev. Sci. Instrum.* **89**, 053505 (2018).
- [7] J.M. McNaney et al, in preparation.
- [8] D.C. Swift et al, in preparation.
- [9] L.H. Thomas, *Proc. Cambridge Phil. Soc.* **23**, 5, 542548 (1927); E. Fermi, *Rend. Accad. Naz. Lincei.* **6**, 602607 (1927).
- [10] R.G. McQueen, S.P. Marsh, J.W. Taylor, J.M. Fritz, and W.J. Carter, in R. Kinslow (Ed.), *High velocity impact phenomena* (Academic, New York, 1970). Data taken from S.P. Marsh (Ed), *LASL Shock Hugoniot Data* (University of California, Berkeley, 1980).
- [11] R.L. Clendenen and H.G. Drickamer, *J. Phys. Chem. Solids* **25**, 865 (1964).
- [12] K.V. Yusenko, S. Khandarkhaeva, T. Fedotenko, A. Pakhomovad, S.A. Gromilov, L. Dubrovinsky, and N. Dubrovinskaia, *J. Alloys and Compounds* **788**, 212 (2019).
- [13] M. Tkacz, *J. Chem. Phys.* **108**, 5, 2084 (1998).
- [14] H. Cynn, J.E. Klepeis, C.-S. Yoo, and D.A. Young, *Phys. Rev. Lett.* **88**, 135701 (2002).
- [15] S.P. Lyon and J.D. Johnson, Los Alamos National Laboratory report LA-UR-92-3407 (1992).
- [16] J.D. Johnson and S.P. Lyon (Los Alamos National Laboratory), documentation for SESAME EOS 3050 (1994).
- [17] R.M. More, K.H. Warren, D.A. Young and G.B. Zimmerman, *Phys. Fluids* **31**, 3059 (1988).
- [18] D.A. Young and E.M. Corey, *J. Appl. Phys.* **78**, 3748 (1995).
- [19] G.S. Tripathi, N.E. Brener, and J. Callaway, *Phys. Rev. B* **38**, 15, 10454 (1988).
- [20] C. Cazorla, D. Alfè, and M.J. Gillan, *Phys. Rev. B* **77**, 224103 (2008).
- [21] C. Cazorla, D. Alfè, and M.J. Gillan, *Comp. Mat. Sci.* **50**, 9, 2732 (2011).
- [22] P. Kumar, N.K. Bhatt, P.R. Vyas, and V.B. Gohel, *Eur. Phys. J. B* **89**, 219 (2016).
- [23] E.L. Pollock and D.M. Ceperley, *Phys. Rev. B* **30**, 2555 (1984).
- [24] For example, L. Collins, I. Kwon, J. Kress, N. Troullier, and D. Lynch, *Phys. Rev. E* **52**, 6202 (1995).
- [25] D.C. Swift, G.J. Ackland, A. Hauer, and G.A. Kyrala, *Phys. Rev. B* **63**, 214107 (2001).
- [26] P. Debye, *Ann. Phys.* **39**, 4, 789839 (1912).
- [27] V.L. Moruzzi, J.F. Janak, and K. Schwarz, *Phys. Rev. B* **37**, 2, 790-799 (1988).
- [28] L.X. Benedict, K.P. Driver, S. Hamel, B. Militzer, T. Qi, A.A. Correa, A. Saul, and E. Schwegler, *Phys. Rev. B* **89**, 224109 (2014).
- [29] K.P. Driver and B. Militzer, *Phys. Rev. E* **95**, 043205 (2017).
- [30] D.C. Swift, T. Lockard, R.G. Kraus, L.X. Benedict, P.A. Sterne, S. Hamel, M. Bethkenhagen, and B.I. Bennett, *Phys. Rev. E* **99**, 063210 (2019).
- [31] D.A. Liberman, *Phys. Rev. B* **20**, 12, 4981 (1979).
- [32] D.A. Liberman and B.I. Bennett, *Phys. Rev. B* **42**, 2475 (1990).
- [33] D.C. Swift, T. Lockard, M. Bethkenhagen, S. Hamel, A. Correa, L.X. Benedict, P.A. Sterne, and B.I. Bennett, submitted and [arXiv:1905.08911](https://arxiv.org/abs/1905.08911), (2019).
- [34] For example, R.F. Smith, J.H. Eggert, R. Jeanloz, T.S. Duffy, D.G. Braun, J.R. Patterson, R.E. Rudd, J. Biener, A.E. Lazicki, A.V. Hamza, J. Wang, T. Braun, L.X. Benedict, P.M. Celliers, and G.W. Collins, *Nature* **511**, 330 (2014).
- [35] D. Fratanduono et al, submitted.
- [36] L.G. Stanton, J.N. Glosli, and M.S. Murillo, *Phys. Rev. X* **8**, 021044 (2018).
- [37] For example, A. Lazicki, J.R. Rygg, F. Coppari, R. Smith, D. Fratanduono, R.G. Kraus, G.W. Collins, R. Briggs, D.G. Braun, D.C. Swift, and J.H. Eggert, *Phys. Rev. Lett.* **115**, 075502 (2015); J. Wang, F. Coppari, R.F. Smith, J.H. Eggert, A.E. Lazicki, D.E. Fratanduono, J.R. Rygg, T.R. Boehly, G.W. Collins, and T.S. Duffy, *Phys. Rev. B* **94**, 104102 (2016).
- [38] D.C. Swift, T. Lockard, R.F. Smith, C.J. Wu, and L.X. Benedict, submitted and [arXiv:1906.04796](https://arxiv.org/abs/1906.04796) (2019).
- [39] P. Hohenberg and W. Kohn, *Phys. Rev. B* **136**, 3B (1964).
- [40] W. Kohn and L.J. Sham, *Phys. Rev.* **140**, 4A (1965).
- [41] J.P. Perdew, J.A. Chevary, S.H. Vosko, K.A. Jackson, M.R. Pederson, D.J. Singh, and C. Fiolhais, *Phys. Rev. B* **46**, 6671 (1992).
- [42] J.A. White and D.M. Bird, *Phys. Rev. B* **50**, R4954 (1994).
- [43] N. Troullier and J.L. Martins, *Phys. Rev. B* **43**, pp 1993-2006 (1991).
- [44] H.J. Monkhorst and J.D. Pack, *Phys. Rev. B* **13**, 5188 (1976).
- [45] M.C. Warren, *Ab initio lattice dynamics and structural phase transitions*, PhD thesis, University of Edinburgh (1997).
- [46] D.C. Swift, D.L. Paisley, K.J. McLellan, and G.J. Ackland, *Phys. Rev. B* **76**, 134111 (2007).
- [47] L. Burakovsky and D.L. Preston, *J. Phys. Chem. Solids* **65**, 1581 (2004).
- [48] V. Ya. Vashchenko and V.N. Zubarev, *Sov. Phys. Solid State* **5**, 653 (1963).
- [49] P. Vinet, J.R. Smith, J. Ferrante, and J.H. Rose, *Phys. Rev. B* **35**, 4, 1945 (1987).
- [50] D.C. Swift et al, in preparation.
- [51] J.D. Johnson and S.P. Lyon (Los Alamos National Laboratory), documentation for SESAME table 33050 (1994).
- [52] C.Y. Ho, R.W. Powell, and P.E. Liley, *J. Phys. Chem. Ref. Data* **3**, supp. 1, 1 (1974).
- [53] F. Simon, and G. Glatzel, *Z. anorg. u. allg. Chem.* **178**, 309 (1929).